

THE CORRELATION BETWEEN DISPERSION MEASURE AND X-RAY COLUMN DENSITY FROM RADIO PULSARS

C. He^{1,2}, C.-Y. Ng^{3,1}, and V. M. Kaspi¹

ncy@bohr.physics.hku.hk

Received _____; accepted _____

¹Department of Physics, McGill University, Montreal, QC H3A 2T8, Canada

²Department of Physics, University of Chicago, Chicago, IL 60637, USA

³Department of Physics, The University of Hong Kong, Pokfulam Road, Hong Kong

ABSTRACT

Pulsars are remarkable objects that emit across the entire electromagnetic spectrum, providing a powerful probe of the interstellar medium. In this study, we investigate the relation between dispersion measure (DM) and X-ray absorption column density N_{H} using 68 radio pulsars detected at X-ray energies with the *Chandra X-ray Observatory* or *XMM-Newton*. We find a best-fit empirical linear relation of $N_{\text{H}} (10^{20} \text{ cm}^{-2}) = 0.30_{-0.09}^{+0.13} \text{ DM (pc cm}^{-3})$, which corresponds to an average ionization of $10_{-3}^{+4}\%$, confirming the ratio of one free electron per ten neutral hydrogen atoms commonly assumed in the literature. We also compare different N_{H} estimates and note that some N_{H} values obtained from X-ray observations are higher than the total Galactic HI column density along the same line of sight, while the optical extinction generally gives the best N_{H} predictions.

Subject headings: dust, extinction — ISM: general — pulsars: general — X-rays: ISM

1. INTRODUCTION

The broadband emission of pulsars from radio frequencies to γ -rays can be used to probe the physical conditions of the interstellar medium (ISM). Specifically, their radio pulsations allow accurate measurements of the free electron column density and their X-ray extinction traces the interstellar gas along the line of sight. Radio waves travelling in the ISM are dispersed by free electrons such that signals at lower frequencies propagate at a lower speed and hence arrive on Earth later than those at higher frequencies. The time delay (Δt) between two observing frequencies (ν_1, ν_2) depends on the dispersion measure (DM), which is the integrated free electron number density n_e from Earth to the source at distance d :

$$\text{DM} = \int_0^d n_e \, dl = \frac{2\pi m_e c}{e^2} \left(\frac{1}{\nu_1^2} - \frac{1}{\nu_2^2} \right)^{-1} \Delta t, \quad (1)$$

where m_e and e are electron mass and charge, respectively, and c is the speed of light. Most free electrons in our Galaxy are found in the hot phase of the ISM, including HII regions ionized by UV radiation from hot O or B type stars and the shock-heated interior of supernova remnants (SNRs). These sources can contribute significant DM up to a few hundred parsecs per cubic centimeter. At X-ray energies, photons are absorbed mostly by heavy elements in the interstellar gas due to the photoelectric effect. This has a strong energy dependence and is most prominent in the soft X-ray band. As a result, it modifies the observed low-energy portion of the X-ray spectrum and has to be accounted for in spectral modeling. The amount of extinction, which is expressed in terms of the equivalent atomic hydrogen column density N_{H} , is sensitive to gas and molecular clouds, which traces the warm and cold phases of the ISM (see Wilms et al. 2000).

One natural question to ask is whether there is any correlation between DM and N_{H} in our Galaxy. Such a correlation can reflect the physical connection between different phases of the ISM. Also, it can provide a useful tool to estimate one quantity from the

other, help plan new observations and determine X-ray luminosity upper limits in cases of non-detection. In the literature, an average ionization fraction of 10% in the ISM, i.e. one free electron per 10 equivalent hydrogen atoms, has been commonly assumed in order to infer N_{H} from DM (e.g., Seward & Wang 1988; Kargaltsev et al. 2007; Gil et al. 2008; Camilo et al. 2012), but the justification for this choice has been unclear. X-ray-emitting radio pulsars offer a powerful diagnostic tool for a quantitative study of the correlation. Because they are model-independent and relatively straightforward to measure from radio timing, DM values are well determined, typically to better than a fractional uncertainty of 10^{-3} . However, what has made the determination of any DM- N_{H} correlation difficult in the past is the lack of high-quality X-ray data for N_{H} measurements. In particular, previous generations of X-ray telescopes had poor angular resolution that precluded discerning the pulsar emission from that of the surrounding SNRs and pulsar wind nebulae (PWNe). Thanks to new X-ray missions such as the *Chandra X-ray Observatory* and *XMM-Newton*, precise measurements of N_{H} have been obtained for many pulsars in recent years, allowing a statistical study of N_{H} values for the first time.

In this paper, we compile a list of DM and N_{H} values for 68 X-ray-emitting radio pulsars using the latest *Chandra* and *XMM-Newton* measurements reported in the literature. We found a clear correlation between these two column densities and obtained a best-fit empirical relation of $10^{+4}_{-3}\%$ ionization. In Section 2, we describe our sample selection criteria. The statistical analysis and results are presented in Section 3, and we discuss the implications of our results in Section 4.

2. SAMPLE SELECTION

We started with a list of X-ray detected radio pulsars from Possenti et al. (2002), Becker & Aschenbach (2002), Pavlov et al. (2007), Kargaltsev & Pavlov (2008), and

Kargaltsev & Pavlov (2010), then expanded the sample through careful literature searches for updated observational results and recent discoveries. The latter include three magnetars that show radio emission (Camilo et al. 2006, 2007; Levin et al. 2010) and over a dozen new pulsars identified in γ -rays with the *Fermi Gamma-ray Space Telescope* and subsequently detected in follow-up radio and X-ray observations (see Marelli et al. 2011). Finally to complete the list, we went through the *Chandra* and *XMM-Newton* data archive to search for pulsar observations, and looked up relevant publications based on these data.

The pulsar DMs are adopted from the ATNF Pulsar Catalog¹ (Manchester et al. 2005). They are all very well measured with negligible uncertainties compared to those for N_{H} . On the other hand, it is much more difficult to determine N_{H} , because this requires a strong X-ray source and good knowledge of the intrinsic emission spectrum. The X-ray emission of pulsars is not fully understood; commonly used models include a blackbody (BB) and a neutron-star hydrogen atmosphere (NSA) for the thermal emission, and a power law (PL) for the non-thermal emission. More complicated models consisting of thermal and non-thermal components are sometimes used. To minimize any bias, we selected the N_{H} values for our sample according to the following criteria:

1. We restricted our choices to those in the latest studies using the *Chandra* and *XMM-Newton* observations, since the good angular resolution and sensitivity of these telescopes offer high-quality spectra with minimal background contamination. Any joint fits with other X-ray telescopes are not considered, in order to avoid cross-calibration uncertainties.
2. We adopted only N_{H} values from actual X-ray spectral fits in which the N_{H} is allowed to vary freely, and ignored any N_{H} inferred from DM, optical extinction (A_{V}), or total

¹<http://www.atnf.csiro.au/research/pulsar/psrcat/>

Galactic HI column density.

3. N_{H} from the best-fit spectral model is always preferred, unless there are physical arguments favoring another model. If different emission models give the same goodness-of-fit and the authors do not indicate a clear preference, we choose the simpler one. For example, we prefer a BB model over an NSA model, since the latter requires more assumptions, including the atmosphere composition, surface magnetic field and gravity.
4. For pulsars associated with bright PWNe, the nebular N_{H} values are adopted if they are better constrained than those of the pulsars, because the simple PL spectra of PWNe can reduce systematic uncertainties in spectral modeling. N_{H} from SNRs are used in a few cases when the pulsars and PWNe are too faint for useful N_{H} measurements.

Our final sample contains 68 pulsars. One of them (PSR B0540–69) is extragalactic and only two (PSRs J1740–5340 and B1821–24) are in globular clusters; cluster pulsars are generally too faint for precise N_{H} measurements. The pulsar DM and N_{H} values are listed in Table 1 and plotted in Figure 1. The reported statistical uncertainties and upper limits for N_{H} are at 90% confidence level, i.e. 1.6σ . We list in the Table the X-ray spectral models used to obtain N_{H} . The choice of spectral model is clear in all cases except PSRs J1622–4950 and B1757–24, for which both thermal and non-thermal fits are acceptable. Nonetheless, N_{H} from different fits only varies by a factor of 2 for J1622–4950 and does not change for B1757–24. Therefore, we conclude that systematic bias induced by spectral models is minimal.

Table 1 also shows the pulsar Galactic coordinates (l , b) and distances, and this information was used to calculate the vertical height (z) from the Galactic Plane. The

coordinates are taken from the ATNF Pulsar Catalog and distance estimates are obtained from parallax measurements, HI absorption measurements of the pulsars or the associated SNRs, or DM using the NE2001 Galactic electron density model (Cordes & Lazio 2002). If available, parallax distances are always preferred since they are the most accurate. All parallax and HI distances are adopted from Verbiest et al. (2012) and references therein, and have been corrected for the Lutz-Kelker bias, except for PSR J1023+0038, which has a recent parallax measurement by Deller et al. (2012). For DM distances, we did not attempt to derive the uncertainties, but note that the fractional uncertainties could be 25% or larger (see e.g., Camilo et al. 2009). Finally, there are exceptional cases in which previous studies argue for different distances than the DM-estimated ones. They are noted in the Table. The pulsar N_{H} and DM are plotted against distance in Figures 2 and 3, respectively.

3. ANALYSIS & RESULTS

Figure 1 shows a positive correlation between the pulsar DM and N_{H} values, with deviations ranging from a factor of a few to an order of magnitude. There are some obvious outliers, including the Vela pulsar (PSR B0833–45), the double pulsar (PSR J0737–3039), and PSR J1747–2809 in the Galactic Center direction. To quantify the DM- N_{H} correlation, we ignored pulsars with N_{H} upper limits and obtained a Pearson’s correlation coefficient of 0.72. This is significant since the one-tailed probability of such a correlation arising by chance from unrelated variables is only 4×10^{-5} . More useful is an empirical relation between these two observables. We performed a linear fit to the data by minimizing the χ^2 value. N_{H} measurements with fractional uncertainties larger than 80% or upper limits only (gray points in Figure 1) are excluded in the fit. We also ignored the Vela pulsar, which is located in the Gum Nebula inside the hot and low-density Local Bubble, and PSR B0540–69, which is in the Large Magellanic Cloud (LMC), because they seem

unlikely to follow the DM- N_{H} correlation as would other Galactic sources. Only statistical uncertainties in N_{H} are considered in the χ^2 -fit since uncertainties in DM are negligible. Also, we did not attempt to model the systematic uncertainties, but we note that the ones introduced by different photoelectric absorption models and elemental abundances, or by cross-calibration between telescopes are only at a few percent level (see Wilms et al. 2000; Tsujimoto et al. 2011), relatively small compared to the statistical uncertainties. Assuming N_{H} and DM are directly proportional, the best fit gives

$$N_{\text{H}} (10^{20} \text{ cm}^{-2}) = 0.30_{-0.09}^{+0.13} \text{ DM (pc cm}^{-3}) , \quad (2)$$

corresponding to an average ionization of $10_{-3}^{+40}\%$. The 90% confidence interval is quoted here, which is obtained from 10000 simulations via bootstrapping resampling (Efron & Tibshirani 1993). The result is plotted in Figure 1. We also tried fitting a more general linear relation by fitting the y-intercept as well, but found that the latter is consistent with zero at 90% confidence. If we ignore the measurement uncertainties in N_{H} and perform a least squares fit, we obtain $N_{\text{H}} (10^{20} \text{ cm}^{-2}) = 0.83 \text{ DM (pc cm}^{-3})$, giving a lower average ionization of 4%.

To check if the DM- N_{H} relation could depend on the source location in the Galaxy, we divided the sample into groups according to their vertical height from the plane and their Galactic longitudes. The results are shown in Figures 1(b) and 1(c), respectively. In the high-DM regime, sources toward the Galactic Center direction, e.g., PSRs J1747–2958 and J1747–2809, show a hint of a larger N_{H} -to-DM ratio. However, the systematic variation is less clear at lower DM and our limited sample precludes a detailed analysis. In Figure 2 we plotted N_{H} against distance. This indicates a general correlation, albeit with a large scatter. There is also a hint that for sources at a similar distance, N_{H} is systematically larger near the Galactic Plane (Figure 2(b)), however, the dependency on Galactic longitude is less clear (Figure 2(c)). The DM variation with distance is presented in Figure 3. While this may seem to exhibit a good correlation at large distances, we note that sources with

DM-derived distances provide no new information, only the NE2001 model prediction. In addition, there is a very large range of DMs for nearby pulsars around 300 pc, from $2.4 \pm 0.2 \text{ pc cm}^{-3}$ for PSR J0108–1431 to $68 \pm 1.6 \text{ pc cm}^{-3}$ for the Vela pulsar, spanning nearly a factor of 30. Similar to N_{H} , Figure 3(b) also indicates a higher DM toward the Galactic Plane.

4. DISCUSSION

We have investigated the DM- N_{H} connection for 68 radio pulsars detected with *Chandra* or *XMM-Newton*. We found a good correlation between these two column densities, suggesting that free electrons in the Galaxy generally trace the interstellar gas. That said, some N_{H} values in Figure 1 show significant deviation from the best-fit line, by a factor of a few up to an order of magnitude. This could be attributed to inhomogeneity of the ISM, possibly due to molecular clouds, supernova remnants, or HII regions in the line of sight. Such an effect is more prominent for nearby sources, since the distribution of free electrons and interstellar gas is highly anisotropic around the Local Bubble (see Taylor & Cordes 1993; Lallement et al. 2003). In particular, there is significant DM contribution from the Gum Nebula (Taylor & Cordes 1993), resulting in a wide range of DMs for pulsars within $\sim 300 \text{ pc}$ (e.g., the Vela pulsar and PSR J0737–3039; see Figure 3). At large distances, local fluctuations are expected to average out and the scatter of N_{H} and DM with respect to distance likely arises from Galactic structure, such as the disk, spiral arms, and different scale heights of various ISM components (see Cox 2005). We have attempted to identify any systematic trends in DM and N_{H} with respect to source location. While Figures 2(b) and 3(b) hint at higher N_{H} and DM toward the Galactic Plane, more sources are needed for a quantitative comparison with the detailed Galactic structure. Beyond our Galaxy, we note that while PSR B0540–69 in the LMC was not used

in the fit, its DM-to- N_{H} ratio lies close to the best-fit line in Figure 1. This is somewhat surprising because of the different interstellar abundances in the LMC than in our Galaxy (Russell & Dopita 1992). We argue that this could merely be a coincidence rather than the general case. Indeed, the LMC contributes 90% of the N_{H} toward PSR B0540–69 (Park et al. 2010) but only two thirds of the DM (Manchester et al. 2006).

The DM- N_{H} correlation can be used to estimate one quantity from the other, offering a useful tool for pulsar observations. For instance, radio pulsations have been claimed from the magnetar 4U 0142+61 with a DM of $27 \pm 5 \text{ pc cm}^{-3}$ (Malofeev et al. 2010). Given its N_{H} value of $9.6 \pm 0.2 \times 10^{21} \text{ cm}^{-2}$ (Göhler et al. 2005), the claimed DM seems somewhat small when compared to other sources of similar N_{H} in Figure 1. For X-ray observations, there are many cases requiring *a priori* knowledge of N_{H} , including flux estimates when planning for new observations, measuring the intrinsic spectra of faint sources, and deriving luminosity limits for non-detection. In many previous studies, N_{H} is inferred from the DM by assuming one free electron per ten neutral hydrogen atoms (e.g. Kargaltsev et al. 2007; Camilo et al. 2012). Our result directly confirms that this is a reasonable approximation, but as a caveat, the scatter in N_{H} is typically a factor of a few up to an order of magnitude.

In addition to DM, the total Galactic HI column density from 21-cm radio surveys (e.g., Kalberla et al. 2005) and A_{V} have also been used as proxies for the X-ray absorption (e.g., Olausen et al. 2013). These N_{H} estimates are plotted in Figure 4. It is clear that some X-ray-inferred N_{H} values exceed the total HI column density of the Galaxy. As shown in the Figure, the latter saturates at $\sim 10^{22} \text{ cm}^{-2}$, resulting in gross underestimates for high-DM ($\gtrsim 100 \text{ pc cm}^{-3}$) or distant ($\gtrsim 3 \text{ kpc}$) pulsars. It has been reported that at high Galactic column densities $\gtrsim 10^{21} \text{ cm}^{-2}$, which occur at low Galactic latitudes, the X-ray absorption columns are generally larger than the HI columns by a factor of 1.5–3 (Arabadjis & Bregman 1999; Baumgartner & Mushotzky 2006). This agrees with our result

and indicates significant X-ray absorption due to molecular clouds rather than neutral hydrogen atoms, hence, the HI column may not be a good tracer for the X-ray absorption.

A_V , on the other hand, is caused by grains of the same heavy elements that give rise to X-ray absorption, therefore, it highly correlates with N_H (e.g., Predehl & Schmitt 1995; Güver & Özel 2009). Given a pulsar’s position and distance, A_V can be estimated from the 3D extinction maps of the Galaxy (e.g., Drimmel et al. 2003), and then N_H can be deduced from the empirical relation $N_H(\text{cm}^{-2}) = 2.21 \times 10^{21} A_V (\text{mag})$ (Güver & Özel 2009). As shown in Figure 4, this method seems to give the best agreement between measured and predicted values, especially for the highest- N_H pulsars. It is worth noting that in some cases DMs were used to infer the pulsar distances, which then give A_V and N_H . This generally provides better results than directly employing the DM- N_H correlation. We believe that this is because the A_V map reflects the distribution of heavy elements in the Galaxy, whereas this crucial information cannot be obtained from DM.

5. CONCLUSION AND OUTLOOK

We have compiled a list of 68 pulsar N_H measurements reported in the literature using *Chandra* and *XMM-Newton* observations, and compared the N_H values with the DMs and distances. Our results show a good correlation between DM and N_H , with a correlation coefficient of 0.72. We obtained an empirical linear relation $N_H (10^{20} \text{ cm}^{-2}) = 0.30_{-0.09}^{+0.13} \text{ DM (pc cm}^{-3})$, implying an average ionization of $10_{-3}^{+4}\%$. This confirms the ratio of one free electron to ten neutral hydrogen atoms commonly used in previous studies. Our finding provides a useful tool to estimate N_H from DM. We compare to other N_H estimates based on the neutral hydrogen column density and A_V , and find that the latter gives the best results, while HI and our empirical DM- N_H relation tend to give underestimates in the high- N_H regime.

The next generation of X-ray missions, including eROSITA (Predehl et al. 2010) and the proposed Neutron Star Interior Composition Explorer (NICER; Gendreau et al. 2012), will significantly expand the pulsar N_{H} sample. In addition, the foreseen Square Kilometer Array (SKA) can provide parallax measurements of a few thousand radio pulsars (Smits et al. 2011). Together these will allow a detailed study of the DM- N_{H} relation in different parts of the Galaxy and its connection with the Galactic structure. In addition to pulsars, it should be possible to compile a database of N_{H} measurements for other Galactic X-ray sources, such as stars, supernova remnants, cataclysmic variables, stellar clusters, white dwarfs, and X-ray binaries, and compare with their distances to build a 3D N_{H} map of our Galaxy.

We thank Oleg Kargaltsev and Slavko Bogdanov for suggesting a list of X-ray-emitting radio pulsars, and Anne Archibald, Antoine Bouchard, and Ryan Lynch for discussion. We acknowledge the anonymous referee for useful suggestions. V.M.K. holds the Lorne Trottier Chair in Astrophysics and Cosmology and a Canadian Research Chair in Observational Astrophysics. This work was supported by NSERC via a Discovery Grant, by FQRNT via the Centre de Recherche Astrophysique du Québec, by CIFAR, and a Killam Research Fellowship.

REFERENCES

- Anderson, G. E., Gaensler, B. M., Slane, P. O., et al. 2012, *ApJ*, 751, 53
- Arabadjis, J. S., & Bregman, J. N. 1999, *ApJ*, 510, 806
- Arzoumanian, Z., Gotthelf, E. V., Ransom, S. M., et al. 2011, *ApJ*, 739, 39
- Baumgartner, W. H., & Mushotzky, R. F. 2006, *ApJ*, 639, 929
- Becker, W., & Aschenbach, B. 2002, in *Neutron Stars, Pulsars, and Supernova Remnants*, ed. W. Becker, H. Lesch, & J. Trümper, 64
- Becker, W., Jessner, A., Kramer, M., Testa, V., & Howaldt, C. 2005, *ApJ*, 633, 367
- Becker, W., Weisskopf, M. C., Tennant, A. F., et al. 2004, *ApJ*, 615, 908
- Bernardini, F., Israel, G. L., Dall’Osso, S., et al. 2009, *A&A*, 498, 195
- Bogdanov, S., Archibald, A. M., Hessels, J. W. T., et al. 2011a, *ApJ*, 742, 97
- Bogdanov, S., & Grindlay, J. E. 2009, *ApJ*, 703, 1557
- Bogdanov, S., van den Berg, M., Heinke, C. O., et al. 2010, *ApJ*, 709, 241
- Bogdanov, S., van den Berg, M., Servillat, M., et al. 2011b, *ApJ*, 730, 81
- Camilo, F., Gaensler, B. M., Gotthelf, E. V., Halpern, J. P., & Manchester, R. N. 2004, *ApJ*, 616, 1118
- Camilo, F., Ng, C.-Y., Gaensler, B. M., et al. 2009, *ApJ*, 703, L55
- Camilo, F., Ransom, S. M., Chatterjee, S., Johnston, S., & Demorest, P. 2012, *ApJ*, 746, 63
- Camilo, F., Ransom, S. M., Halpern, J. P., & Reynolds, J. 2007, *ApJ*, 666, L93

- Camilo, F., Ransom, S. M., Halpern, J. P., et al. 2006, *Nature*, 442, 892
- Caswell, J. L., McClure-Griffiths, N. M., & Cheung, M. C. M. 2004, *MNRAS*, 352, 1405
- Chang, C., Pavlov, G. G., Kargaltsev, O., & Shibano, Y. A. 2012, *ApJ*, 744, 81
- Claussen, M. J., Wilking, B. A., Benson, P. J., et al. 1996, *ApJS*, 106, 111
- Cognard, I., Guillemot, L., Johnson, T. J., et al. 2011, *ApJ*, 732, 47
- Cordes, J. M., & Lazio, T. J. W. 2002, *astro-ph/0207156*
- Cox, D. P. 2005, *ARA&A*, 43, 337
- De Luca, A., Caraveo, P. A., Mereghetti, S., Negroni, M., & Bignami, G. F. 2005, *ApJ*, 623, 1051
- Deller, A. T., Archibald, A. M., Briske, W. F., et al. 2012, *ApJ*, 756, L25
- Drimmel, R., Cabrera-Lavers, A., & López-Corredoira, M. 2003, *A&A*, 409, 205
- Durant, M., Kargaltsev, O., Pavlov, G. G., et al. 2012, *ApJ*, 746, 6
- Efron, B., & Tibshirani, R. J. 1993, *An Introduction to the Bootstrap* (Chapman & Hall/CRC)
- Freedman, W. L., Madore, B. F., Gibson, B. K., et al. 2001, *ApJ*, 553, 47
- Gaensler, B. M., Arons, J., Kaspi, V. M., et al. 2002, *ApJ*, 569, 878
- Gaensler, B. M., van der Swaluw, E., Camilo, F., et al. 2004, *ApJ*, 616, 383
- Gendreau, K. C., Arzoumanian, Z., & Okajima, T. 2012, *Proc. SPIE*, 8443, 13
- Gil, J., Haberl, F., Melikidze, G., et al. 2008, *ApJ*, 686, 497

- Göhler, E., Wilms, J., & Staubert, R. 2005, *A&A*, 433, 1079
- Gonzalez, M. E., Kaspi, V. M., Pivovarov, M. J., & Gaensler, B. M. 2006, *ApJ*, 652, 569
- Gotthelf, E. V., Helfand, D. J., & Newburgh, L. 2007, *ApJ*, 654, 267
- Guillemot, L., Johnson, T. J., Venter, C., et al. 2012, *ApJ*, 744, 33
- Güver, T., & Özel, F. 2009, *MNRAS*, 400, 2050
- Halpern, J. P., Gotthelf, E. V., Leighly, K. M., & Helfand, D. J. 2001, *ApJ*, 547, 323
- Harris, W. E. 1996, *AJ*, 112, 1487
- Hinton, J. A., Funk, S., Carrigan, S., et al. 2007, *A&A*, 476, L25
- Holler, M., Schöck, F. M., Eger, P., et al. 2012, *A&A*, 539, A24
- Hughes, J. P., Slane, P. O., Park, S., Roming, P. W. A., & Burrows, D. N. 2003, *ApJ*, 591, L139
- Hui, C. Y., Huang, R. H. H., Trepl, L., et al. 2012, *ApJ*, 747, 74
- Kalberla, P. M. W., Burton, W. B., Hartmann, D., et al. 2005, *A&A*, 440, 775
- Kargaltsev, O., Durant, M., Misanovic, Z., & Pavlov, G. G. 2012, *Science*, 337, 946
- Kargaltsev, O., Misanovic, Z., Pavlov, G. G., Wong, J. A., & Garmire, G. P. 2008, *ApJ*, 684, 542
- Kargaltsev, O., & Pavlov, G. G. 2007, *ApJ*, 670, 655
- Kargaltsev, O., & Pavlov, G. G. 2008, in *AIP Conf. Proc.*, Vol. 983, 40 Years of Pulsars: Millisecond Pulsars, Magnetars and More, ed. C. Bassa, Z. Wang, A. Cumming, & V. M. Kaspi (Melville, NY: AIP), 171

- Kargaltsev, O., & Pavlov, G. G. 2010, in AIP Conf. Proc., Vol. 1248, X-ray Astronomy 2009; Present Status, Multi-Wavelength Approach and Future Perspectives (Melville, NY: AIP), 25
- Kargaltsev, O., Pavlov, G. G., & Garmire, G. P. 2007, ApJ, 660, 1413
- Kargaltsev, O., Pavlov, G. G., & Wong, J. A. 2009, ApJ, 690, 891
- Kaspi, V. M., Gotthelf, E. V., Gaensler, B. M., & Lyutikov, M. 2001, ApJ, 562, L163
- Lallement, R., Welsh, B. Y., Vergely, J. L., Crifo, F., & Sfeir, D. 2003, A&A, 411, 447
- LaMassa, S. M., Slane, P. O., & de Jager, O. C. 2008, ApJ, 689, L121
- Levin, L., Bailes, M., Bates, S., et al. 2010, ApJ, 721, L33
- Li, X. H., Lu, F. J., & Li, T. P. 2005, ApJ, 628, 931
- Malofeev, V. M., Teplykh, D. A., & Malov, O. I. 2010, Astronomy Reports, 54, 995
- Manchester, R. N., Fan, G., Lyne, A. G., Kaspi, V. M., & Crawford, F. 2006, ApJ, 649, 235
- Manchester, R. N., Hobbs, G. B., Teoh, A., & Hobbs, M. 2005, AJ, 129, 1993
- Marelli, M. 2012, PhD thesis, University of Insubria
- Marelli, M., De Luca, A., & Caraveo, P. A. 2011, ApJ, 733, 82
- Maselli, A., Cusumano, G., Massaro, E., et al. 2011, A&A, 531, A153
- Matheson, H., & Safi-Harb, S. 2010, ApJ, 724, 572
- McGowan, K. E., Zane, S., Cropper, M., Vestrand, W. T., & Ho, C. 2006, ApJ, 639, 377
- Misanovic, Z., Pavlov, G. G., & Garmire, G. P. 2008, ApJ, 685, 1129

- Negueruela, I., Ribó, M., Herrero, A., et al. 2011, *ApJ*, 732, L11
- Ng, C.-Y., Kaspi, V. M., Ho, W. C. G., et al. 2012, *ApJ*, 761, 65
- Ng, C.-Y., Roberts, M. S. E., & Romani, R. W. 2005, *ApJ*, 627, 904
- Ng, C.-Y., Romani, R. W., Briskin, W. F., Chatterjee, S., & Kramer, M. 2007, *ApJ*, 654, 487
- Ng, C.-Y., Kaspi, V. M., Dib, R., et al. 2011, *ApJ*, 729, 131
- Olausen, S. A., Zhu, W. W., Vogel, J. K., et al. 2013, *ApJ*, 764, 1
- Pancrazi, B., Webb, N. A., Becker, W., et al. 2012, *A&A*, 544, A108
- Park, S., Hughes, J. P., Slane, P. O., Mori, K., & Burrows, D. N. 2010, *ApJ*, 710, 948
- Pavlov, G. G., Chang, C., & Kargaltsev, O. 2011, *ApJ*, 730, 2
- Pavlov, G. G., Kargaltsev, O., & Briskin, W. F. 2008, *ApJ*, 675, 683
- Pavlov, G. G., Kargaltsev, O., Garmire, G. P., & Wolszczan, A. 2007, *ApJ*, 664, 1072
- Posselt, B., Arumugasamy, P., Pavlov, G. G., et al. 2012a, *ApJ*, 761, 117
- Posselt, B., Pavlov, G. G., Manchester, R. N., Kargaltsev, O., & Garmire, G. P. 2012b, *ApJ*, 749, 146
- Possenti, A., Cerutti, R., Colpi, M., & Mereghetti, S. 2002, *A&A*, 387, 993
- Possenti, A., Rea, N., McLaughlin, M. A., et al. 2008, *ApJ*, 680, 654
- Predehl, P., & Schmitt, J. H. M. M. 1995, *A&A*, 293, 889
- Predehl, P., Andritschke, R., Böhringer, H., et al. 2010, *Proc. SPIE*, 7732, 23

- Ransom, S. M., Ray, P. S., Camilo, F., et al. 2011, *ApJ*, 727, L16
- Rea, N., McLaughlin, M. A., Gaensler, B. M., et al. 2009, *ApJ*, 703, L41
- Reid, I. N., & Gizis, J. E. 1998, *AJ*, 116, 2929
- Renaud, M., Marandon, V., Gotthelf, E. V., et al. 2010, *ApJ*, 716, 663
- Roberts, D. A., Goss, W. M., Kalberla, P. M. W., Herbstmeier, U., & Schwarz, U. J. 1993, *A&A*, 274, 427
- Romani, R. W., Ng, C.-Y., Dodson, R., & Briskin, W. 2005, *ApJ*, 631, 480
- Romani, R. W., Shaw, M. S., Camilo, F., Cotter, G., & Sivakoff, G. R. 2010, *ApJ*, 724, 908
- Russell, S. C., & Dopita, M. A. 1992, *ApJ*, 384, 508
- Schöck, F. M., Büsching, I., de Jager, O. C., Eger, P., & Vorster, M. J. 2010, *A&A*, 515, A109
- Seward, F. D., & Wang, Z.-R. 1988, *ApJ*, 332, 199
- Shelton, R. L., Kuntz, K. D., & Petre, R. 2004, *ApJ*, 611, 906
- Smits, R., Tingay, S. J., Wex, N., Kramer, M., & Stappers, B. 2011, *A&A*, 528, A108
- Taylor, J. H., & Cordes, J. M. 1993, *ApJ*, 411, 674
- Temim, T., Slane, P., Reynolds, S. P., Raymond, J. C., & Borkowski, K. J. 2010, *ApJ*, 710, 309
- Tepedelenliǧlu, E., & Ögelman, H. 2007, *ApJ*, 658, 1183
- Trimble, V. 1973, *PASP*, 85, 579
- Tsujimoto, M., Guainazzi, M., Plucinsky, P. P., et al. 2011, *A&A*, 525, A25

- Van Etten, A., Romani, R. W., & Ng, C.-Y. 2008, *ApJ*, 680, 1417
- Verbiest, J. P. W., Weisberg, J. M., Chael, A. A., Lee, K. J., & Lorimer, D. R. 2012, *ApJ*, 755, 39
- Webb, N. A., Olive, J.-F., & Barret, D. 2004, *A&A*, 417, 181
- Weisskopf, M. C., Tennant, A. F., Yakovlev, D. G., et al. 2011, *ApJ*, 743, 139
- Wilms, J., Allen, A., & McCray, R. 2000, *ApJ*, 542, 914
- Zavlin, V. E. 2006, *ApJ*, 638, 951
- Zavlin, V. E., & Pavlov, G. G. 2004, *ApJ*, 616, 452
- Zhu, W. W., Kaspi, V. M., McLaughlin, M. A., et al. 2011, *ApJ*, 734, 44

Table 1. DM, N_{H} , and Distances for the 68 Pulsars Used in This Study

PSR	DM (pc cm ⁻³)	N_{H} (10 ²⁰ cm ⁻²)	Distance ^a (kpc)	l (deg)	b (deg)	z^b (pc)	Model ^c	Ref.
J0030+0451	4.333±0.001	2.2±1.0	0.28 ^{+0.10} _{-0.06} P	113.1	-57.6	-236	NSA×3	1
J0108-1431	2.4 ± 0.2	2 ± 2	0.21 ^{+0.09} _{-0.05} P	140.9	-76.8	-205	BB	2
B0136+57	73.779±0.006	50 ± 3	2.6 ^{+0.3} _{-0.2} P	129.2	-4.0	-183	PL	3
J0205+6449	140.7±0.3	41.6 ^{+0.8} _{-0.7}	3.2 ^o	130.7	+3.1	+172	PL+RS (SNR)	4, 5
J0218+4232	61.252±0.005	8 ± 4	2.67 ^d	139.5	-17.5	-804	PL	6
B0355+54	57.1420±0.0003	60 ± 30	1.0 ^{+0.2} _{-0.1} P	148.2	+0.8	+14	PL (PWN)	7
J0437-4715	2.64476±0.00007	0.25 ^{+0.40} _{-0.24}	0.156 ± 0.001 ^P	253.4	-42.0	-104	PL+NSA×2	8
B0531+21 (Crab)	56.791±0.001	32±2	2.00 ^o	184.6	-5.8	-202	PL	9, 10
J0538+2817	39.570±0.001	25 ± 2	1.3 ± 0.2 ^P	179.7	-1.7	-38	BB	11
B0540-69	146.6 ± 0.2	67 ± 5	50 ^o	279.7	-31.5	-26137	PL (SNR)	12, 13
B0628-28	34.468±0.017	6 ⁺⁵ ₋₃	0.32 ^{+0.05} _{-0.04} P	237.0	-16.8	-92.3	PL	14
B0656+14	13.977±0.013	4.3±0.2	0.28 ± 0.03 ^P	201.1	+8.3	+40	PL+BB×2	15
J0737-3039	48.920±0.005	< 1	1.1 ^{+0.2} _{-0.1} P	245.2	-4.5	-86	BB×2	16
B0823+26	19.454±0.004	< 14	0.32 ^{+0.08} _{-0.05} P	197.0	+31.7	+168	PL	17
B0833-45 (Vela)	67.99±0.01	1.6 ^{+0.3} _{-0.2}	0.28 ± 0.02 ^P	263.6	-2.8	-14	PL (PWN)	18
B0950+08	2.958±0.003	3.2±1.3	0.261±0.005 ^P	228.9	+43.7	+180	PL+BB	19
J1016-5857	394.2±0.2	50±30	8.00 ^d	284.1	-1.9	-263	PL	20
J1023+0038	14.325±0.010	< 9	1.37±0.04 ^P	243.5	+45.8	+980	PL+NSA	21
J1024-0719	6.48520±0.00008	2 ⁺³ ₋₂	0.49 ^{+0.12} _{-0.08} P	251.7	+40.5	+318	BB	22
B1046-58	129.1±0.2	90 ⁺⁶⁰ ₋₃₀	2.9 ^{+1.2} _{-0.7} h	287.4	+0.6	+29	PL	23
B1055-52	30.1±0.5	2.7 ± 0.2	0.72 ^d	286.0	+6.7	+84	PL+BB×2	15
J1119-6127	707.4±1.3	200 ⁺⁵⁰ ₋₄₀	8.4±0.4 ^o	292.2	-0.5	-78.7	PL+BB	24, 25
J1124-5916	330±2	31±6	5 ⁺³ ₋₂ h	292.0	+1.8	+153	PL	26
J1231-1411	8.090±0.001	< 5	0.44 ^d	295.5	+48.4	+329	NSA+PL	27
B1259-63	146.72±0.03	25 ⁺⁶ ₋₅	2.3±0.4 ^o	304.2	-1.0	-40	PL	28, 29
J1357-6429	128.5±0.7	37 ⁺²⁰ ₋₁₃	2.50 ^d	309.9	-2.5	-110	PL (PWN)	30
J1400-6325	563±4	209 ± 20	11.27 ^d	310.6	-1.6	-313	PL (PWN)	31
J1420-6048	358.8±0.2	540 ⁺³⁵⁰ ₋₂₇₀	5.61 ^d	313.5	+0.2	+22	PL (PWN)	32
B1451-68	8.6±0.2	17 ⁺⁴⁰ ₋₁₇	0.43 ^{+0.06} _{-0.05} P	313.9	-8.5	-64	PL+BB	33
J1509-5850	140.6±0.8	210 ⁺⁷⁰ ₋₂₀	2.62 ^d	320.0	-0.6	-28	PL (PWN)	34
B1509-58	252.5±0.3	115±5 ^d	4.4 ^{+1.3} _{-0.8} h	320.3	-1.2	-89	PL (PWN)	35

Table 1—Continued

PSR	DM (pc cm ⁻³)	N_{H} (10 ²⁰ cm ⁻²)	Distance ^a (kpc)	l (deg)	b (deg)	z^b (pc)	Model ^c	Ref.
J1550–5418	830±50	410±10	9.55 ^d	327.2	−0.1	−22	PL+BB	36
J1614–2230	34.4865±0.0001	20 ⁺²² _{−11}	1.27 ^d	352.6	+20.2	+438	BB×2	37
J1617–5055	467±5	345±20	6.82 ^d	332.5	−0.3	−33	PL	38
J1622–4950	820±30	540 ⁺¹⁶⁰ _{−140}	8.73 ^d	333.8	−0.1	−16	BB	39
B1706–44	75.69±0.05	50±6	2.6 ^{+0.5h} _{−0.6}	343.1	−2.7	−122	PL (PWN)	40
J1718–3718	371.1±1.7	130±30	6.6 ^d	349.8	+0.2	+25	BB	41
J1718–3825	247.4±0.3	72 ⁺⁵⁰ _{−13}	3.6 ^d	349.0	−0.4	−27	PL (PWN)	42
J1734–3333	578±9	70 ⁺⁴⁰ _{−30}	6.46 ^d	354.8	−0.4	−49	BB	43
J1740–5340	71.8±0.2	22 ± 4	2.7±0.2 ^o	338.2	−12.0	−560	PL	44, 45
J1740+1000	23.85±0.05	10 ± 2	1.24 ^d	34.0	+20.3	+430	PL+BB	46
J1741–2054	4.7±0.1	15±5	0.38 ^d	6.4	+4.9	+33	PL (PWN)	47
J1747–2809	1133±3	2300±150	13.31 ^d	0.9	+0.1	+18	PL (PWN)	48
J1747–2958	101.5±1.6	270±10	5 ^o	359.3	−0.8	−73	PL (PWN)	49, 50
B1757–24	289±10	350 ⁺¹³⁰ _{−110}	5.22 ^d	5.3	−0.9	−80	PL	51
B1800–21	233.99±0.05	138 ⁺⁶⁰ _{−35}	3.88 ^d	8.4	+0.2	+10	PL (PWN)	52
J1809–1917	197.1±0.4	71 ⁺⁶⁰ _{−40}	3.55 ^d	11.1	+0.1	+5	PL	53
J1809–1943	178±5	72±3	3.6 ± 0.5 ^h	10.7	−0.2	−10	BB×3	54
J1819–1458	196.0±0.4	60±30	3.55 ^d	16.0	+0.1	+5	BB	55
B1821–24	120.502±0.002	26 ± 2	5.5±0.3 ^o	7.8	−5.6	−535	PL	56, 57
B1823–13	231±1	120 ⁺⁶⁰ _{−80}	3.93 ^d	18.0	−0.7	−47	PL (PWN)	58
J1833–1034	169.5±0.1	224 ⁺⁹ _{−10}	4.5 ± 0.5 ^h	21.5	−0.9	−70	PL	59
B1853+01	96.74±0.12	120±16	3 ^o	34.6	−0.5	−26	VNEI×2 (SNR)	60, 61
J1930+1852	308±4	195±4	7 ^{+3h} _{−2}	54.1	+0.3	+32	PL (PWN)	62
B1929+10	3.180±0.004	1.7 ^{+2.3} _{−1.7}	0.31 ^{+0.09p} _{−0.06}	47.4	−3.9	−21	PL+BB	63
B1937+21	71.0398±0.0002	97 ± 24	5 ^{+2p} _{−1}	57.5	−0.3	−25	PL	64
B1951+32	45.006±0.0190	30 ± 2	3 ± 2 ^h	68.8	+2.8	+148	PL	65
B1957+20	29.1168±0.0007	16 ± 10	2.49 ^d	59.2	−4.7	−204	PL	66
J2021+3651	368±1	67 ⁺⁸ _{−7}	12.19 ^d	75.2	+0.1	+24	PL	67
J2022+3842	429.1±0.5	160±30	10 ^o	76.9	+1.0	+168	PL	68
J2032+4127	114.8±0.1	48 ⁺¹³ _{−15}	3.65 ^d	80.2	+1.0	+66	PL	69
J2043+2740	21.0±0.1	< 50	1.8 ^d	70.6	−9.2	−286	BB	17

Table 1—Continued

PSR	DM (pc cm ⁻³)	N_{H} (10 ²⁰ cm ⁻²)	Distance ^a (kpc)	l (deg)	b (deg)	z^b (pc)	Model ^c	Ref.
J2124–3358	4.601±0.003	3±2	0.30 ^{+0.07} _{-0.05} ^p	10.9	–45.4	–214	PL+BB	22
B2224+65	36.079±0.009	25 ⁺¹⁶ ₋₁₁	1.86 ^d	108.6	+6.8	+222	PL	70
J2229+6114	204.97±0.02	30 ⁺⁹ ₋₄	3 ⁺⁵ ₋₁ ^o	106.6	+2.9	+154	PL	71, 72
J2241–5236	11.41085±0.00003	< 25	0.51 ^d	337.5	–54.9	–417	PL	69
J2302+4442	13.762±0.006	2 ⁺³¹ ₋₂	1.18 ^d	103.4	–14.0	–286	NSA	73
B2334+61	58.410±0.015	26 ⁺²⁶ ₋₅	3.15 ^d	114.3	+0.2	+13	BB	74

^aDistance estimates are either parallax or H I absorption measurements adopted from Verbiest et al. (2012) and Deller et al. (2012) or from the DM using the NE2001 model (Cordes & Lazio 2002). They are denoted by the letters p, h, and d, respectively. We did not attempt to quantify the uncertainties in the DM distances. The designation “o” indicates distance estimates based on other arguments; see the references for details.

^bVertical distance from the Galactic Plane calculated using the source distance and Galactic latitude b .

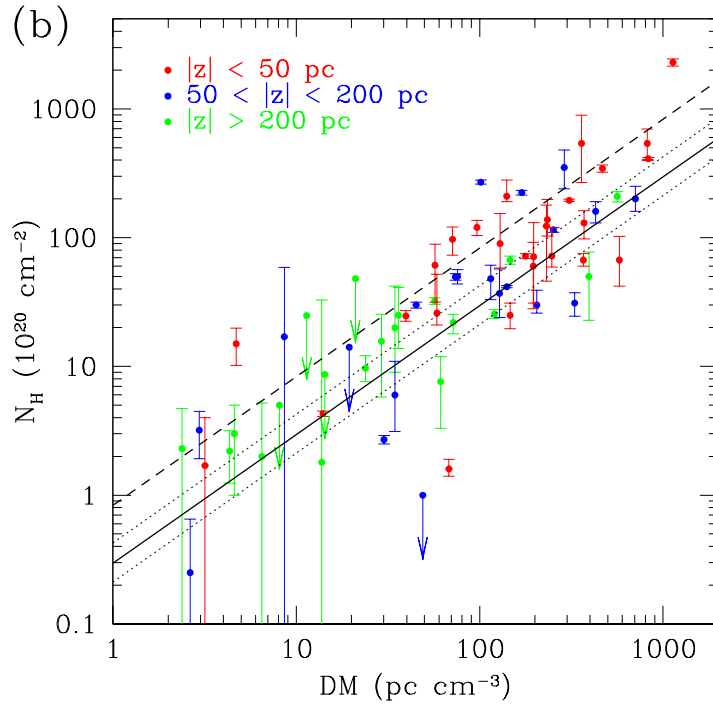
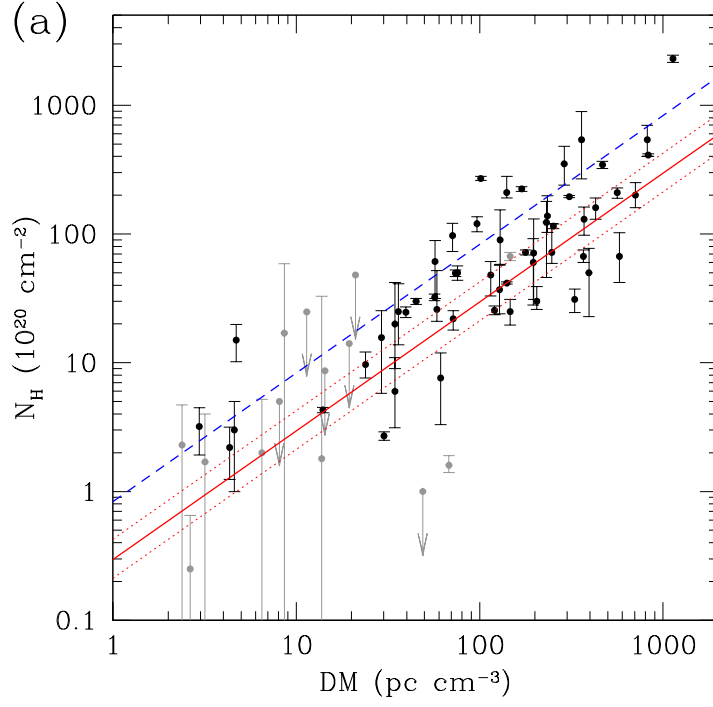
^cSpectral models used to obtain N_{H} : blackbody (BB), power law (PL), and neutron star atmosphere (NSA). N_{H} values determined from the associated SNRs or PWNe are noted. The SNR spectra were fitted with Raymond-Smith (RS) and non-equilibrium ionization (VNEI) models.

^dSchöck et al. (2010) reported $N_{\text{H}} = 1.15 \times 10^{21} \text{ cm}^{-2}$, but mentioned that it is consistent with the previous result from Gaensler et al. (2002), which gave $N_{\text{H}} = 9.5 \times 10^{21} \text{ cm}^{-2}$. Therefore, the former is assumed to be a typographical error and we adopt the value $1.15 \times 10^{22} \text{ cm}^{-2}$.

Note. — Uncertainties and upper limits on N_{H} are all scaled to the 90% confidence level, i.e. 1.6σ .

References. — (1) Bogdanov & Grindlay 2009; (2) Posselt et al. 2012a; (3) Maselli et al. 2011; (4) Gotthelf et al. 2007; (5) Roberts et al. 1993; (6) Webb et al. 2004; (7) Tepedelenliđlu & Ögelman 2007; (8) Durant et al. 2012; (9) Weisskopf et al. 2011; (10) Trimble 1973; (11) Ng et al. 2007; (12) Park et al. 2010; (13) Freedman et al. 2001; (14) Becker et al. 2005; (15) De Luca et al. 2005; (16) Possenti et al. 2008; (17) Becker et al. 2004; (18) LaMassa et al. 2008; (19) Zavlin & Pavlov 2004; (20) Camilo et al. 2004; (21) Bogdanov et al. 2011a; (22) Zavlin 2006; (23) Gonzalez et al. 2006; (24) Ng et al. 2012; (25) Caswell et al. 2004; (26) Hughes et al. 2003; (27) Ransom et al. 2011; (28) Pavlov et al. 2011; (29) Negueruela et al. 2011; (30) Chang et al. 2012; (31) Renaud et al. 2010; (32) Ng et al. 2005; (33) Posselt et al. 2012b; (34) Kargaltsev et al. 2008; (35) Schöck et al. 2010; (36) Ng et al. 2011; (37) Pancrazi et al. 2012; (38) Kargaltsev et al. 2009; (39) Anderson et al. 2012; (40) Romani et al. 2005; (41) Zhu et al. 2011; (42) Hinton et al. 2007; (43) Olausen et al. 2013; (44) Bogdanov et al. 2010; (45) Reid & Gizis

1998; (46) Kargaltsev et al. 2012; (47) Romani et al. 2010 (48) Holler et al. 2012; (49) Gaensler et al. 2004; (50) Gaensler et al. 2004; (51) Kaspi et al. 2001; (52) Kargaltsev et al. 2007; (53) Kargaltsev & Pavlov 2007; (54) Bernardini et al. 2009; (55) Rea et al. 2009; (56) Bogdanov et al. 2011b; (57) Harris 1996; (58) Pavlov et al. 2008; (59) Matheson & Safi-Harb 2010; (60) Shelton et al. 2004; (61) Claussen et al. 1996; (62) Temim et al. 2010; (63) Misanovic et al. 2008; (64) Ng et al. 2013, in preparation; (65) Li et al. 2005; (66) Guillemot et al. 2012; (67) Van Etten et al. 2008; (68) Arzoumanian et al. 2011; (69) Marelli 2012; (70) Hui et al. 2012; (71) Marelli et al. 2011; (72) Halpern et al. 2001; (73) Cognard et al. 2011; (74) McGowan et al. 2006



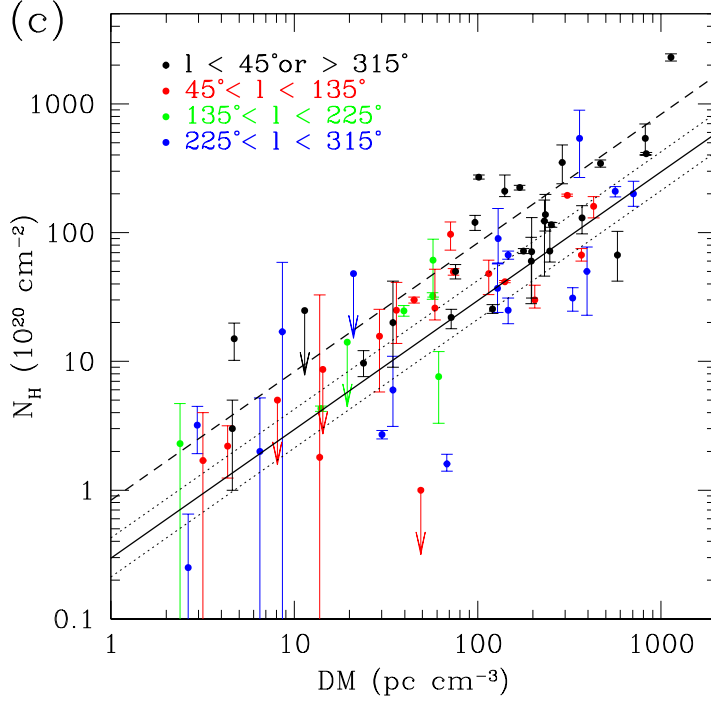
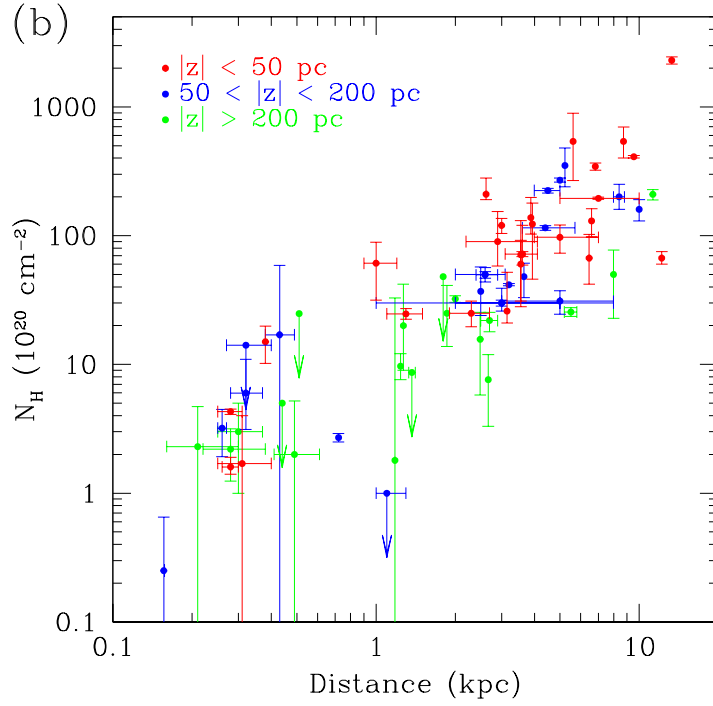
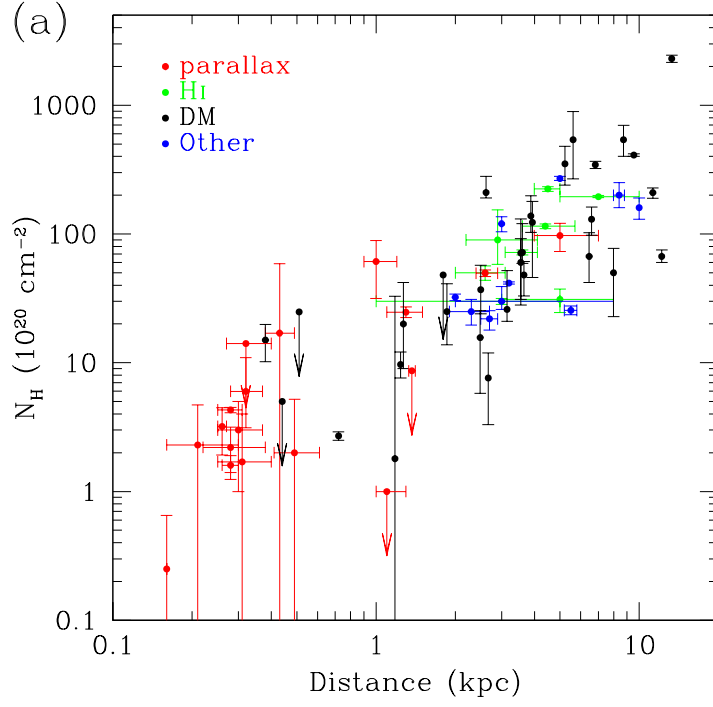


Fig. 1.— N_{H} versus DM for 68 pulsars. (a) Data points in gray color, including the Vela pulsar, PSR B0540–69, and N_{H} measurements with fractional uncertainties larger than 80% or only upper limits are not used in the fit. The red solid and dotted lines show the best linear fit with the 90% confidence interval, and the blue dashed line is the same fit ignoring measurement uncertainties. These correspond to $10^{+4}_{-3}\%$ and 4% ionization, respectively. Uncertainties in DM are negligible. The same plot is shown in (b) and (c) with different color schemes, indicating the pulsar vertical distance from the Galactic Plane and their Galactic longitudes, respectively.



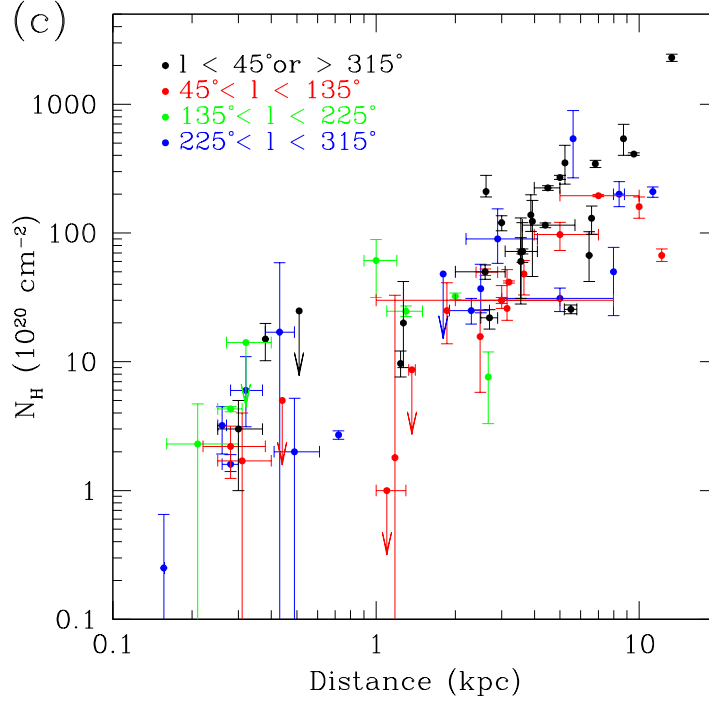
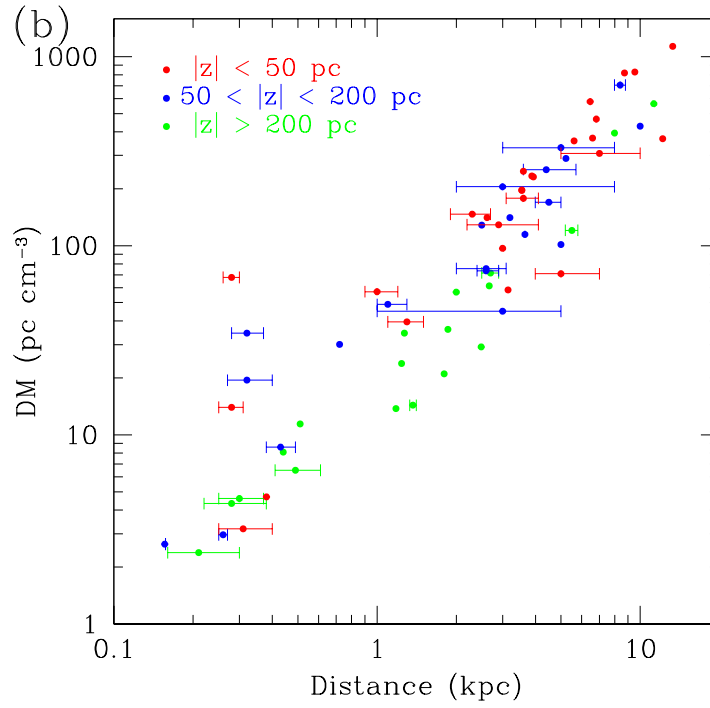
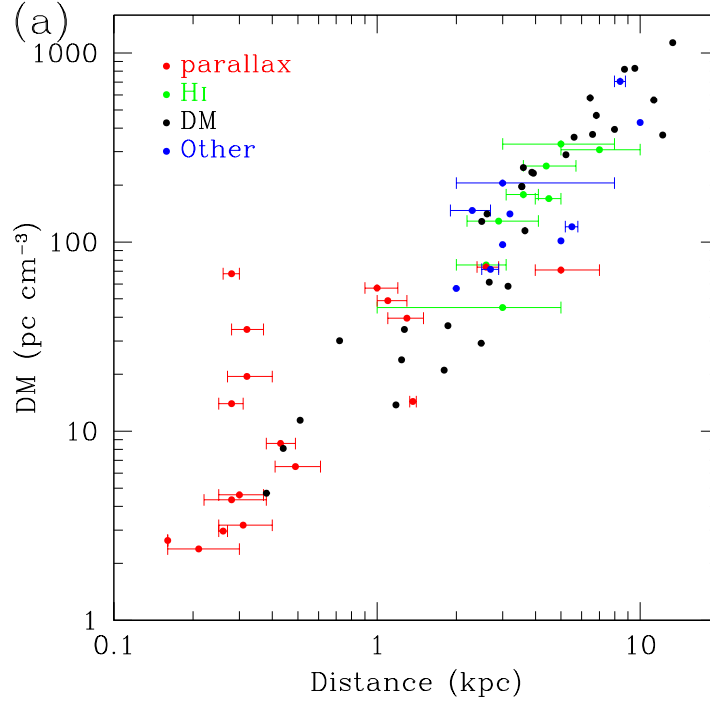


Fig. 2.— N_H versus distance for Galactic pulsars. PSR B0540–69 is not shown here. (a) The colors indicate different types of distance measurement. We did not estimate the uncertainties for the DM distances. The same plot with different color schemes is shown in (b) and (c), indicating the pulsar vertical distance from the Galactic Plane and their Galactic longitudes, respectively.



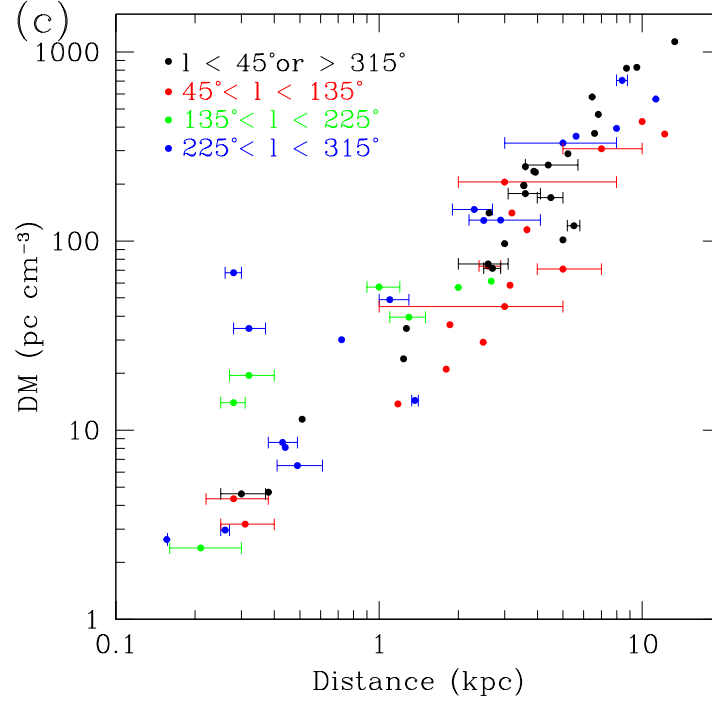
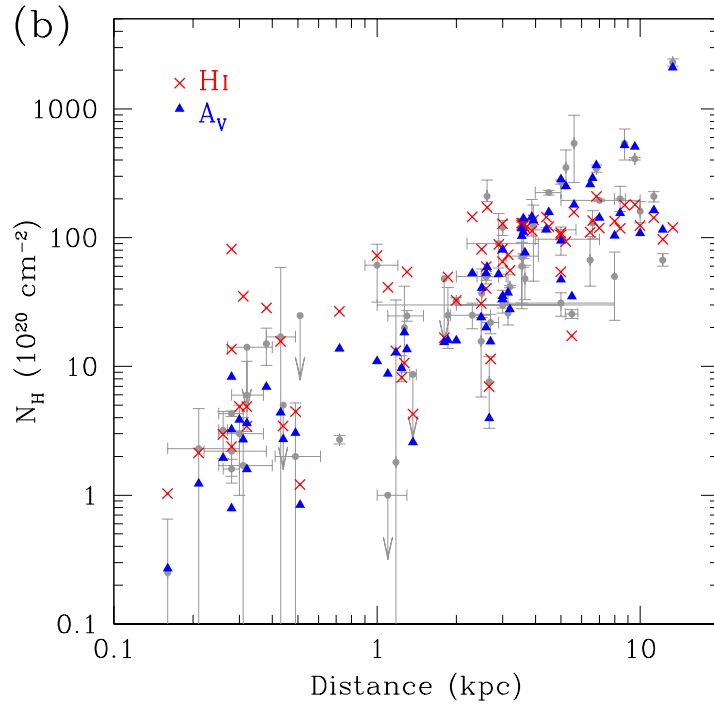
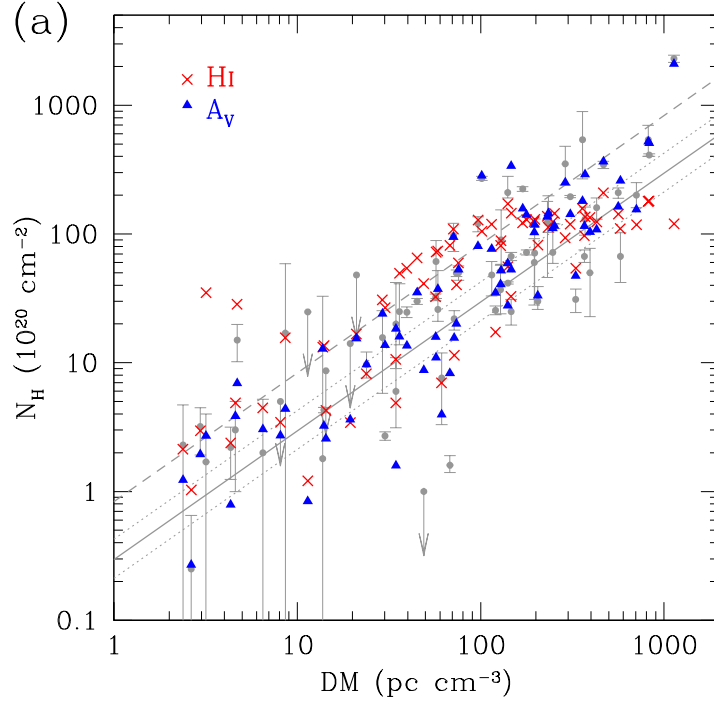


Fig. 3.— Same as Figure 2, but for DM versus distance. Uncertainties in DM are not plotted, as they are smaller than the data points.



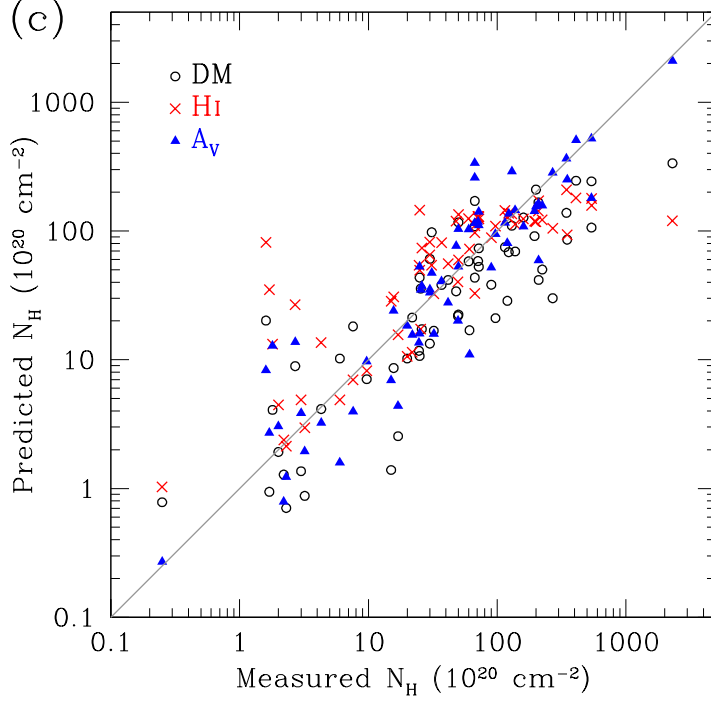


Fig. 4.— Comparison between N_H estimates and measurements. The underlying plots in (a) and (b) are the same as Figures 1 and 2, respectively. The red crosses indicate the total line-of-sight Galactic HI column densities for each pulsar, given by 21 cm radio observations (Kalberla et al. 2005). The blue triangles show estimates based on A_V (see text). In (c), the open circles represent predictions from our best-fit DM- N_H relation.